

Spectroscopy of the frustrated quantum antiferromagnet Cs_2CuCl_4

We investigate the electronic structure of Cs_2CuCl_4 , a material discussed in the framework of a frustrated quantum antiferromagnet, by means of resonant inelastic x-ray scattering (RIXS) and Density Functional Theory (DFT). From the non-dispersive highly localized dd excitations, we resolve the crystal field splitting of the Cu^{2+} ions in a strongly distorted tetrahedral coordination. This allows us to model the RIXS spectrum within the Crystal Field Theory (CFT), assign the dd orbital excitations and retrieve experimentally the values of the crystal field splitting parameters D_q , D_s and D_τ . The electronic structure obtained *ab-initio* agrees with the RIXS spectrum and modelled by CFT, highlighting the potential of combined spectroscopic, cluster and DFT calculations to determine the electronic ground state of complex materials.

I. INTRODUCTION

Geometrically frustrated spin textures are excellent candidates to search for new forms of exotic magnetism, like quantum spin liquids [1] and topological magnetic ordering [2]. The magnetic order and its excitations, resulting from the geometrically frustrated triangular, Kagomé or honeycomb lattices are the focus of current and intense research [3]. This rich phenomenology is also a manifestation of the interplay between multiple energy scales - magnetic exchange, Coulomb interaction, orbital excitations and crystal field splitting, Δ^{CF} , as has been observed in the cubic vanadates [4] and superconducting cuprates [5].

Among the solids showing frustrated magnetism Cs_2CuCl_4 has attracted great attention. Below the Néel temperature $T_N = 0.61$ K, Cs_2CuCl_4 shows a long-range antiferromagnetic (AF) order with an incommensurate spiral wave vector. Between T_N and the Curie temperature $T_C = 2.65$ K, a spin-liquid phase with strong in-chain spin correlations has been discussed by means of specific heat [6] and electron spin resonance (ESR) [7]. Neutron scattering [8] experiments have uncovered an extensive two-spinon continuum and revealed a weaker interchain exchange coupling, $J'/k_B = 1.4$ K, between Cu atoms than the intrachain interaction, $J/k_B = 4.7$ K, along b axis [9], as depicted in Fig. 1(a). In addition, interlayer coupling in Cs_2CuCl_4 is smaller than J and J' by more than one order of magnitude, $J'' = 0.13$ K, in good agreement with the theoretical description of a quasi-1D weakly coupled $S=1/2$ Heisenberg chain [10].

A quantitative description of spin exchange interactions in frustrated magnets, as in Cs_2CuCl_4 , requires a precise knowledge of the crystal-field ground state (Δ^{CF}) and electron-orbital excitations. However, the determination of the orbital ground state, the value of Δ^{CF} and the Jahn-Teller distortion (Δ^{JT}) of the tetrahedrally coordinated Cu^{2+} ions in Cs_2CuCl_4 are still missing and their relationship with the magnetic anisotropy ($J \approx 3 \times J'$) needs further study. Experimentally, inelastic neutron scattering [11, 12] and x-ray absorption spectroscopy (XAS) [13] have been used to study the magnitude of the crystal field splitting and the dd orbital excitations, but the information is sometimes hampered by phonons, small amount of crystals or by the metal-ligand hybridization. Theoretically, *ab initio* density functional

theory (DFT) methods provide only a single-electron approximation of excited states, often in disagreement with experimental spectroscopic measurements. This is further complicated by strong quantum fluctuations, associated with spin-1/2 degrees of freedom in the highly localized regime and geometrical frustration that can give rise to entangled quantum phases. Interestingly, changes in the symmetry of the occupied orbitals and large orbital dispersions have been observed in several cuprates [14, 15] and titanates [16] in the energy range between 0.5-2 eV by means of resonant inelastic x-ray scattering (RIXS). On the other side, the study of orbital excitations in non-oxide materials is rather scarce and the consequences for the physics of quasi one dimensional systems are less explored.

Here, we have carried out a comprehensive spectroscopic and theoretical study of the quantum antiferromagnet Cs_2CuCl_4 by means of RIXS, DFT and cluster calculations. We have been able to resolve the crystal field splitting, and show that the dd orbital excitations are well modeled assuming a strongly distorted tetrahedral symmetry with crystal field parameters $D_q = -0.120$ eV, $D_s = 0.085$ eV and $D_\tau = -0.165$ eV. Moreover, despite the strong hybridization between the Cu^{2+} and Cl^- ions, we find that the RIXS spectra describes a strongly ionic character of Cu-Cl bond, which may explain the absence of dispersion of the dd excitations. On a broader picture, our results exemplify how RIXS, DFT and cluster calculations can be combined to study the ground state of complex materials.

II. EXPERIMENTAL AND COMPUTATIONAL METHODS

Single crystals of Cs_2CuCl_4 were grown by slow evaporation at 300 K from an acidic (HCl) solution containing a 2:1 stoichiometric ratio of the CsCl and $\text{CuCl}_2 \cdot \text{H}_2\text{O}$. The quality of the single crystals was checked by x-ray diffraction, resulting in lattices parameters $a = 9.77$ Å, $b = 7.61$ Å, $c = 12.41$ Å, and Raman scattering [17]. DFT calculations [18, 19] were performed using the all-electron, full-potential WIEN2K code [20] based on the augmented plane wave plus local orbital (APW+lo) basis set [21]. The generalized gradient approximation (GGA) in the Perdew-Burke-Ernzerhof [22] scheme was used for the ex-

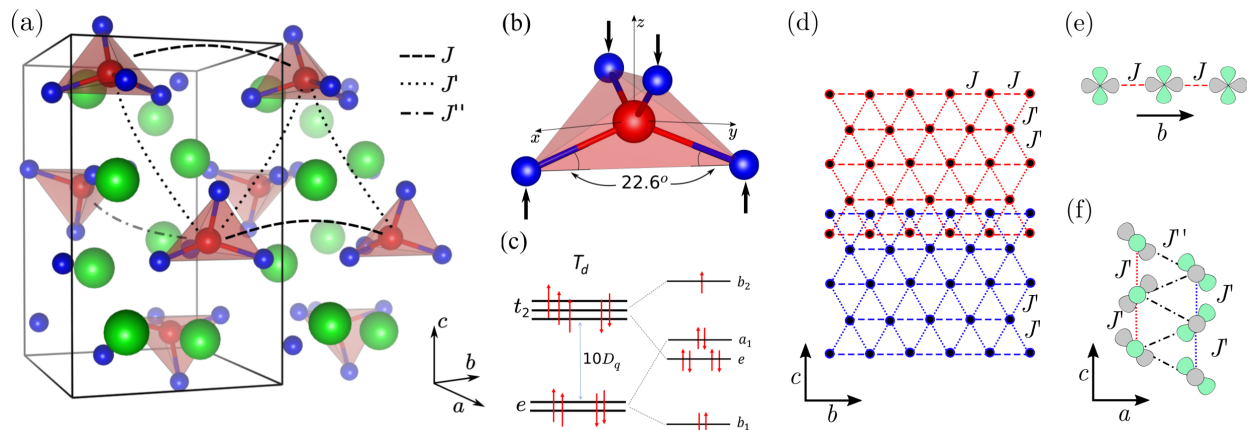


FIG. 1. (a) Orthorhombic unit cell of Cs_2CuCl_4 . Green, red and blue balls denote Cs, Cu and Cl atoms, respectively. The tetrahedral coordination of Cu is highlighted. The intrachain J (dashed), the interchain J' (dotted) and the interplane J'' (dot-dashed) magnetic exchange interactions have been depicted. Notice the triangular layers formed by the J and J' interactions. These are schematically shown in panel (d). Notice also the quasi-1D Heisenberg chains along the b axis formed by the J interactions. This is better seen in panel (e). (b) Locally distorted tetrahedral environment of Cu atom. Black arrows along the z -direction represent the distortion of the tetrahedron to a square planar situation. The Cl-Cu-Cl angles have been represented to denote the highly distorted scenario. (c) Crystal field splitting of the Cu^{2+} ions in the distorted tetrahedral environment, where the e orbitals lower their energy with respect to the t_2 . The Jahn-Teller distortion further splits the energy levels with b_1 ($d_{x^2-y^2}$), e (d_{xz}/d_{yz}), a_1 (d_{z^2}) and b_2 (d_{xy}) symmetries. Their relation to the crystal field parameters D_q , D_s and D_τ is provided by eq. (1). (d) Representation of two planes, red and blue, each of them defined by the J and J' exchange constants. The sites where the magnetic moments lay are represented as black dots. (e) Schematic of the 1D-Heisenberg chain along the b axis defined by the J couplings. A direct overlap between the b_2 (d_{xy}) orbitals (depicted in green and grey) can be seen in this direction. (f) Schematic of the J' and J'' couplings. Note how the b_2 orbital coupled by J' are tilted 90° from one chain to the other along the c axis. A more complex interplane geometry can be seen along the a axis.

change correlation functional, with a fully converged k -mesh of $R_{mt}K_{max}=7.0$ and muffin-tin radii of 2.5, 2.22, 1.91 a.u. for Cs, Cu and Cl, respectively. RIXS experiments were performed at the U41-PEAXIS beamline at BESSY II at 20 K and combined energy resolution, $\Delta E \approx 150$ meV. To minimize the elastic background, the measurements were carried out with horizontal polarization and the scattering angle 2θ was set to 110° . The elastic (zero-energy loss) peak position was determined from the elastic scattering spectra of carbon tape. The Cs_2CuCl_4 crystal was plate-like with a flat surface normal to the (010) direction.

III. RESULTS AND DISCUSSION

The crystal structure of Cs_2CuCl_4 is orthorhombic with space group $Pnma$. Each Cu^{2+} atom is surrounded by 4 Cl^- ions in a distorted tetrahedral coordination (Fig. 1(a)), with Cu-Cl bond length of 2.25\AA , and Cl-Cu-Cl angle of 22.6° , smaller than the perfect tetrahedral value of 45° , Fig. 1(b), due to the large distortion of the tetrahedron towards a square planar scenario. As shown in Fig. 1(c), the tetrahedral environment splits the d -levels into low energy 2-fold e and high energy 3-fold degenerate t_2 orbitals (Fig. 1(c)), which are further Jahn-Teller distorted towards a lower symmetry, D_{2d} point

group [23]. This chemical environment provides a spatially anisotropic spin-1/2 triangular antiferromagnet of Cu-Cl chains on a geometrical bc plane, bonded by Cl^- ions along the a direction. Magnetic susceptibility, showing no trace of magnetic order down to 5 K (not shown), is in good agreement with a weakly frustrated magnet [24].

Figure 2 summarizes the DFT results of the electronic structure of Cs_2CuCl_4 for the simple unit cell depicted on Fig. 1(a). This structure leads to a ferromagnetic state, since there is only one non-equivalent Cu atom. Calculations assuming a non-magnetic ground state severely underestimate the charge gap and directly give a metallic solution. We have found that calculations on a $1 \times 2 \times 1$ supercell provide an antiferromagnetic order as the lowest energy solution for the ground state, in agreement with the previous report of Foyevtsova et al. [25]. However, both magnetic orders lead to the same electronic energy levels, and consequently to the same energy gaps. Therefore, this guarantees that the ferromagnetic solution can be used to analyze the electronic spectrum of Cs_2CuCl_4 . The usage of the ferromagnetic state entails several advantages for the analysis of the spectrum. First, it makes the calculation computationally affordable, especially for the wannierization that will be carried out. A reduction of the Bloch subspace from 136 to 68 bands is achieved when considering the ferromagnetic state instead of the

antiferromagnetic one. Apart from that, the ferromagnetic solution allows for a better visualization of the Cu spin state, due to the asymmetric spin channel band occupation. This allows a direct comparison between the crystal field splitting (Fig. 1c), the DFT band structure (Fig. 2b) and the RIXS spectrum (Fig. 4b).

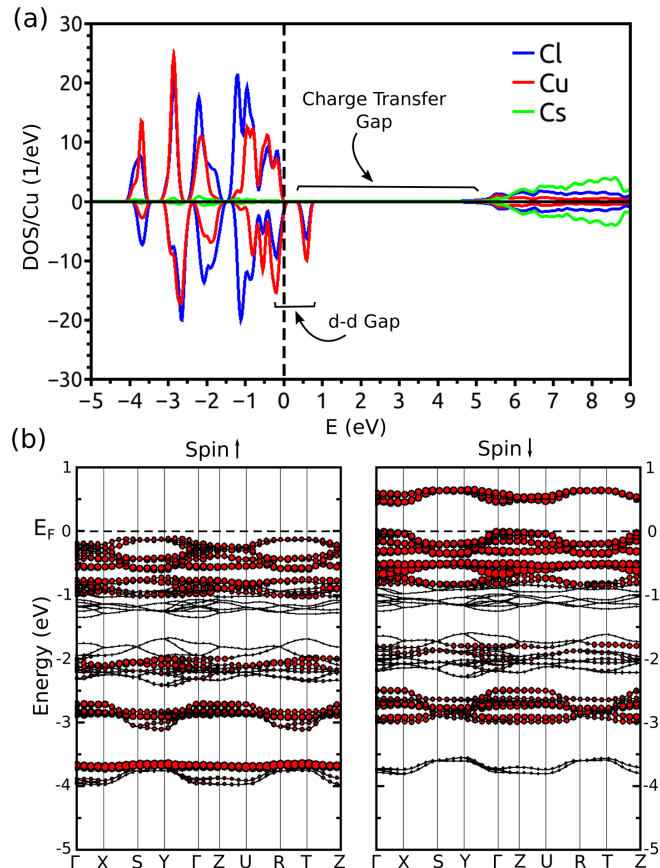


FIG. 2. Summary of the DFT calculations (a) Projected density of states (DOS) for the ferromagnetic structure of Cs_2CuCl_4 , Cs (Cu, Cl) atom in green (red, blue). Both charge transfer and dd energy gaps have been highlighted. (b) Energy bands for the majority (minority) spin channel on the left (right) panel. The d -orbital character of the Cu atom is depicted as red circles.

Between -4 and 0 eV (Fig. 2(a)) the density of states (DOS) shows a strong Cu $3d$ and Cl $3p$ character, while the Cs bands do not contribute at the Fermi level and, therefore, do not hybridize with the CuCl_4 cluster. The Cu and Cl bands are separated from the next unoccupied states by a gap of 4.5 eV, having mostly Cs character. We call this charge transfer gap and corresponds to the energy difference between the CuCl_4 cluster and the Cs ions. On the other hand, the dd gap appears below 1 eV and represents the energy gap between the Fermi level and the empty d_{xy} orbital. Figure 2(b) delves into the band structure of Cs_2CuCl_4 . Bonding and antibonding bands show up between -4 and -3 eV and -1 and 1 eV,

respectively. Moreover, our calculations predict a spin $1/2$ for the Cu atoms resulting from the asymmetric spin channel occupation. It can be clearly seen in Fig. 2b that the minority spin channel undergoes a shift towards higher energies. Whether this shift is a consequence of the Coulomb repulsion or the exchange interactions cannot be determined from our analysis. However, considering that the exchange interaction is one order of magnitude smaller than Coulomb repulsion, this could be the dominant term in the substantial energy shift we found in our calculations.

Having carried out a theoretical description of the electronic structure of Cs_2CuCl_4 , we proceed with the analysis of the RIXS spectra. The fast improvement of the RIXS instrumentation in energy resolution of soft x-ray RIXS has allowed the study of the low energy electronic properties of correlated systems, giving detailed information of collective magnetic, charge and orbital excitations [26]. Figure 3(b) illustrates the case of the Cu^{2+} ion with a $3d^9$ electronic configuration in a tetrahedral crystal field (T_d), with a hole in a $|xy\rangle$ state. In the initial step of RIXS, an x-ray photon excites a $2p_{3/2}$ electron from the ground state, $|i\rangle$, into the $3d$ shell (intermediate state, $|n\rangle$) filling the $|xy\rangle$ orbital and creating an excited core-hole state. This process corresponds to the x-ray absorption, XAS, at 931.5 eV (black curve in figure 3a). In the final step ($|f\rangle$), the core hole is annihilated via decay towards the ground state (elastic scattering, $E_{\text{loss}}=0$ eV) or an excited state (magnons, phonons, dd transitions) [27].

Figure 3(c) displays the incident energy (E_{in}) vs energy loss (E_{loss}) RIXS map. The maximum intensity of the resonant features is observed at $E_{\text{in}}=931$ eV (Fig. 3(d)), 0.5 eV below the maximum of the L_3 absorption edge (Figure 3(a)). In nice agreement with the DFT calculations, the charge transfer excitations resulting from the CuCl_4 cluster to the Cs $6s$ states are observed as a broad band at $E_{\text{loss}}=4$ eV, matching the optical gap observed by absorption spectroscopy [28]. As shown in the inset of Fig. 3(d), this charge transfer gap displays 2 broad bands at 3.7 and 4.2 eV, corresponding to transitions from the Fermi level and the d_{xy} orbital above the Fermi level (Fig. 2(b)) to the upper Cs $6s$ bands. The region between $E_{\text{loss}}=0.5-1.2$ eV corresponds to the optically forbidden crystal field dd excitations, as widely reported in superconducting cuprates [26], and identified in the DFT calculations below 1 eV. The orbital assignment of these excitations was verified by comparing their energy with the DFT calculations. Since the $3d$ and $3p$ bands of Cu and Cl atoms are disentangled in energy from the rest (Fig. 2(b)), an expansion of the Bloch manifold can be performed in real space in terms of *localized Wannier functions* [29]. A symmetry analysis of those Wannier functions allows to identify how the crystal field splitting affects the Cu $3d$ orbitals.

In a tetrahedral coordination, the $3d^9$ electronic configuration split the crystal field generated by Cl ions surrounding a Cu^{2+} ion into the energetically lower Cu e

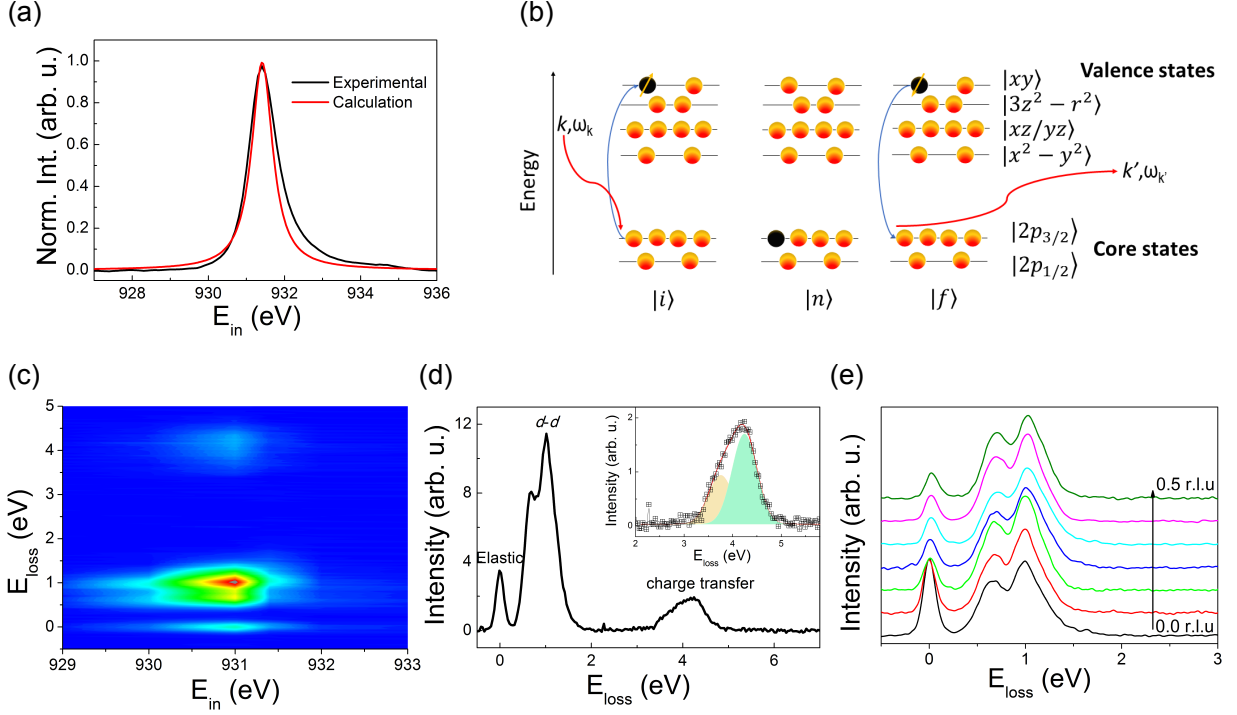


FIG. 3. (a) Experimental (black) and calculated (red) x-ray absorption (XAS) of Cs_2CuCl_4 . (b) Schematics of the RIXS process showing the initial, intermediate and final steps. (c) RIXS map plotting the energy loss, E_{loss} , against the incoming energy, E_{in} , for Cs_2CuCl_4 at 20 K. The maximum intensity of the inelastic features appears at $E_{\text{in}}=931$ eV. (d) Close up view of the RIXS scan at $E_{\text{in}}=931$ eV, highlighting the elastic, dd excitations and the charge gap in the inset. (e) In-plane momentum dependence of the dd excitations, showing no orbital dispersion.

doublet and higher Cu t_2 triplet. Owing to the Jahn-Teller uniaxial distortion of the tetrahedron, the t_2 triplet is further split into the doubly degenerated d_{xz}/d_{yz} states (e irreducible representation) and the half-filled d_{xy} states (b_2), and the degenerate $d_{x^2-y^2}$ (b_1) and d_{z^2} (a_1) become also energetically non-equivalent (Fig. 1(c)). The values of the crystal field splitting describing the tetrahedral distortion, D_q , D_τ and D_s , are related to the on-site orbital energies through:

$$\begin{aligned}
 a_1 &= 6D_q - 2D_s - 6D_\tau \\
 b_1 &= 6D_q + 2D_s - D_\tau \\
 b_2 &= -4D_q + 2D_s - D_\tau \\
 e &= -4D_q - 2D_s + 4D_\tau
 \end{aligned}
 \tag{1}$$

As shown in Fig. 1(c), we found that the b_1 and the b_2 orbitals correspond to the lowest and highest energy levels, respectively. Apart from that, the strong orthorhombic distortion of the tetragonal environment inverts the energy levels of the doubly degenerated e and a_1 .

To better understand the dd excitations in the RIXS spectra, we adopt the *hole* language, where the ground state represents a hole in the b_2 orbital, hence, an e orbital excitation corresponds to moving a hole from the b_2 to the e orbital. Therefore, the dd transitions in

Cs_2CuCl_4 originate from the decay of an electron from the b_1 , a_1 and e orbitals due to the broken degeneracy of the 3d states. Within the energy resolution of our experimental setup, we can discriminate the 3 orbital intratomic transitions; 2 sharp excitations at 0.67 and 1.02 eV, respectively, and a shoulder at 1.21 eV (see Fig. 4(b)). Having considered only the tetrahedral point group, T_d , this would result in a crystal field splitting Δ_t of 1.2 eV, a rather high value assuming $\Delta_t \approx 0.44\Delta_{Oh}$. However, this number is a direct consequence of the strongly distorted tetrahedra towards a square planar geometry (see figure 1(b)), which increases the splitting of the energy levels, since $\Delta_{sp} \approx 1.74\Delta_{Oh}$. Further, we detect no orbital dispersion (Fig. 3(e)) indicating highly localized orbital excitations. Since these dd excitations are intra-atomic and well localized, they can be simulated within a full-multiplet calculation considering a single site of a Cu^{2+} ions of the D_{4h} point group, isomorphic with the D_{2d} [30], which is exemplified by a regular tetrahedron elongated along one of its C_2 axes. The RIXS simulations were carried out with the exact diagonalization code Quanty [31, 32] including the Coulomb interactions and multiplet effects. We have adopted the $U_{pd}/U_{dd}=1.2$ ratio for the Coulomb repulsion [33, 34] and all atomic parameters were taken 80% of the atomic Hartree-Fock values to compensate the ab-

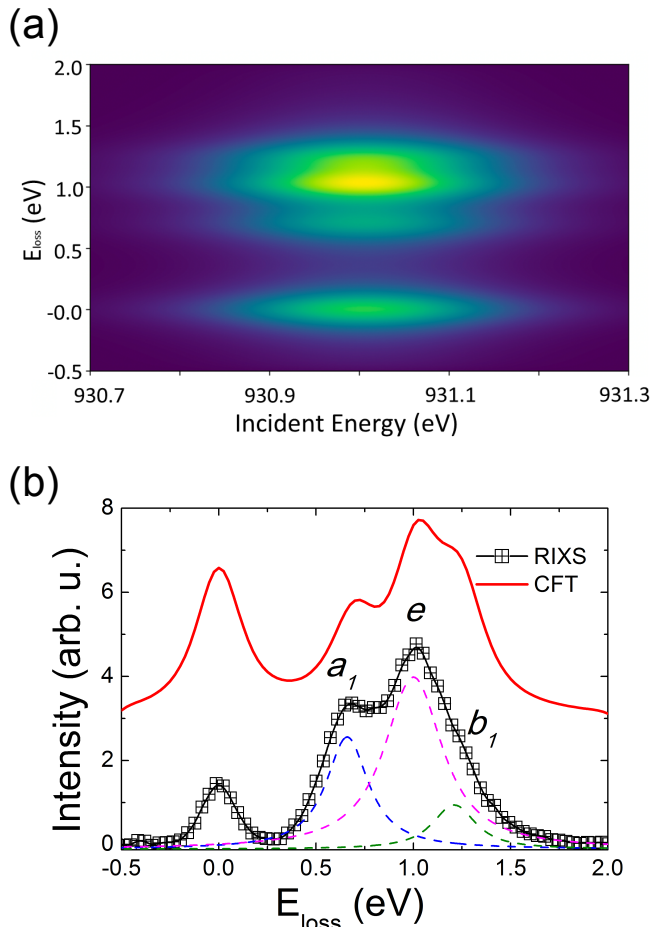


FIG. 4. (a) Calculated RIXS intensity map within the CFT theory, highlighting the crystal field excitations. (b) Comparison of the experimental and theoretical RIXS spectrum for 931 eV incident energy. Labeled are the dd transitions. The calculated RIXS spectrum is vertically shifted for clarity.

sorption effects of the configuration interaction, leaving the radial integrals D_q , D_s and D_τ , as input parameters in the calculation. The 3 orbital transitions corresponding to the b_1 , a_1 and doubly degenerated e orbitals are clearly identified in the calculated RIXS map of figure 4(a). As shown in Fig. 4(b), the experimental RIXS spectrum is fairly well reproduced with an additional instrumental and experimental broadening of 0.1 and 0.25 eV, respectively. From the simulation, we obtain $D_q = -0.120$ eV, $D_s = 0.085$ eV and $D_\tau = -0.165$ eV. The same sign of D_q and D_τ indicates an axial elongation and, therefore, a proximity to a square planar geometry. The negative values of D_q and D_τ account for the stabilization of the b_1 state as the lowest level followed by the e doublet, in agreement with the *wannierization* of the DFT bands. Moreover, the value of D_s shows that the a_1 level shifts its energy resulting in the splitting scheme depicted in figure 1(c). The ground state is 2-

fold degenerate with spin and orbital quantum numbers $\langle S_z \rangle = \pm 1/2$ and $\langle L_z \rangle = \pm 0.31$ and orbital occupations $N_{\text{Cu}} = 9.0$ and $N_{\text{Cl}} = 6.0$ electrons, which agree with the strong ionic character of the Cu^{2+} and Cl^- bond. Moreover, the Quanyty simulation of the XAS spectrum using the same atomic Hartree-Fock and crystal field parameters is rather satisfactory (Figure 3(a)).

As shown in the Introduction in Fig. 1, the half filled b_2 orbital gives a straightforward explanation of the low temperature antiferromagnetism and magnetic anisotropy revealed by electron spin resonance (ESR) and neutron scattering [9]. We can see in Fig. 1e that the intrachain J coupling has a direct overlap between the neighbouring b_2 orbital along the b axis. However, for the interchain neighbours defined by J' , we can see that the b_2 orbitals of different chains are tilted (Fig. 1f). This explains the observation of a stronger intrachain (along the b axis) than interchain exchange coupling, $J' \approx J/3$. The tilting of the b_2 orbitals between different planes, as well as the larger separation between this kind of neighbours, agrees with the small exchange coupling observed for J'' .

On the other hand, following theoretical predictions [35, 36], the observation of spin-orbital separation concentrated first on systems with orbital degeneracy [14, 37] and revealed a sizable and asymmetric coupling between orbital and spin degrees of freedom in systems with antiferromagnetic correlations. This coupling leads to the confinement of orbital excitations in magnetic systems with higher dimensions as reported in CaCu_2O_3 [15], where magnetic correlations are still nearly one-dimensional. Therefore, the small exchange coupling energies and the directed character of the orbital motion along the chains would favor the dispersion of orbital excitations in Cs_2CuCl_4 . Besides, the local coupling of Jahn-Teller effect and lattice vibrations seems to be responsible for the absence of orbital waves in the 3D orbital ordered system KCuF_3 [38], despite of the Ising-like anisotropy in the short range order region [39]. Indeed, the Jahn-Teller effect is responsible for the high energy dd orbital excitations but, to the best of our knowledge, no orbital ordering was observed in Cs_2CuCl_4 . Therefore, relying on the directional character of electron hopping and the resulting one-dimensionality of orbital motion, the observation of collective orbital excitations in Cs_2CuCl_4 could be restricted to one orbital of particular symmetry and fall below the two-spinon continuum or limited by the instrumental resolution.

IV. CONCLUSIONS

In conclusion, we have carried out a comprehensive spectroscopic study of the geometrically frustrated quantum spin liquid Cs_2CuCl_4 , achieving a good agreement between experiments, cluster calculations and density functional theory. We have obtained the values of D_q , D_s and D_τ that fairly reproduce the RIXS spectrum and

shown that the *charge transfer gap*, commonly seen in the RIXS experiments, corresponds here to the energy gap between the CuCl_4 cluster and the Cs s states. Moreover, the possible reason for the lack of an orbiton dispersion might be the strong ionic character of the Cu-Cl bond,

unlike the orbiton dispersion observed in cuprates with a high degree of covalency [14, 15] or the low resolution of our instrumental setup.

We acknowledge Y. Lu and Justina Schlappa for fruitful discussions and critical reading of the manuscript.

-
- [1] Savary, L.; Balents, L. *Reports on Progress in Physics* **2016**, *80*, 016502.
- [2] Fert, A.; Reyren, N.; Cros, V. *Nature Reviews Materials* **2017**, *2*, 17031.
- [3] Takagi, H.; Takayama, T.; Jackeli, G.; Khaliullin, G.; Nagler, S. E. *Nature Reviews Physics* **2019**, *1*, 264–280.
- [4] Khaliullin, G.; Horsch, P.; Oleś, A. M. *Phys. Rev. Lett.* **2001**, *86*, 3879–3882.
- [5] Keimer, B.; Kivelson, S. A.; Norman, M. R.; Uchida, S.; Zaanen, J. *Nature* **2015**, *518*, 179–186.
- [6] Tokiwa, Y.; Radu, T.; Coldea, R.; Wilhelm, H.; Tyliczynski, Z.; Steglich, F. *Phys. Rev. B* **2006**, *73*, 134414.
- [7] Zvyagin, S. A.; Kamenskyi, D.; Ozerov, M.; Wosnitzer, J.; Ikeda, M.; Fujita, T.; Hagiwara, M.; Smirnov, A. I.; Soldatov, T. A.; Shapiro, A. Y.; Krzystek, J.; Hu, R.; Ryu, H.; Petrovic, C.; Zhitomirsky, M. E. *Phys. Rev. Lett.* **2014**, *112*, 077206.
- [8] Coldea, R.; Tennant, D. A.; Tsvetik, A. M.; Tyliczynski, Z. *Phys. Rev. Lett.* **2001**, *86*, 1335–1338.
- [9] Coldea, R.; Tennant, D. A.; Tyliczynski, Z. *Phys. Rev. B* **2003**, *68*, 134424.
- [10] Starykh, O. A.; Katsura, H.; Balents, L. *Phys. Rev. B* **2010**, *82*, 014421.
- [11] Xiao, Y.; Zbiri, M.; Downie, R. A.; Bos, J.-W. G.; Brückel, T.; Chatterji, T. *Phys. Rev. B* **2013**, *88*, 214419.
- [12] Babkevich, P.; Finco, A.; Jeong, M.; Dalla Piazza, B.; Kovacevic, I.; Klughertz, G.; Krämer, K. W.; Kraemer, C.; Adroja, D. T.; Goremychkin, E.; Unruh, T.; Strässle, T.; Di Lieto, A.; Jensen, J.; Rønnow, H. M. *Phys. Rev. B* **2015**, *92*, 144422.
- [13] Butorin, S. M.; Kvashnina, K. O.; Vegelius, J. R.; Meyer, D.; Shuh, D. K. *Proceedings of the National Academy of Sciences* **2016**, *113*, 8093–8097.
- [14] Schlappa, J. et al. *Nature* **2012**, *485*, 82–85.
- [15] Bisogni, V.; Wohlfeld, K.; Nishimoto, S.; Monney, C.; Trinckauf, J.; Zhou, K.; Kraus, R.; Koepf, K.; Sekar, C.; Strocov, V.; Büchner, B.; Schmitt, T.; van den Brink, J.; Geck, J. *Phys. Rev. Lett.* **2015**, *114*, 096402.
- [16] Ulrich, C.; Ament, L. J. P.; Ghiringhelli, G.; Braicovich, L.; Moretti Sala, M.; Pezzotta, N.; Schmitt, T.; Khaliullin, G.; van den Brink, J.; Roth, H.; Lorenz, T.; Keimer, B. *Phys. Rev. Lett.* **2009**, *103*, 107205.
- [17] Jara, E.; Barreda-Argüeso, J. A.; González, J.; Rodríguez, F.; Valiente, R. *Phys. Rev. B* **2019**, *99*, 134106.
- [18] Hohenberg, P.; Kohn, W. *Phys. Rev.* **1964**, *136*, B864.
- [19] Jones, R. O.; Gunnarsson, O. *Rev. Mod. Phys.* **1989**, *61*, 689.
- [20] Schwarz, K.; Blaha, P. *Comp. Mat. Sci.* **2003**, *28*, 259–273.
- [21] Sjöstedt, E.; Nördstrom, L.; Singh, D. J. *Solid State Commun.* **2000**, *114*, 15.
- [22] Perdew, J. P.; Burke, K.; Ernzerhof, M. *Phys. Rev. Lett.* **1996**, *77*, 3865–3868.
- [23] Lamba, O.; Sinha, S. *Solid State Communications* **1986**, *57*, 365 – 371.
- [24] Zheng, W.; Singh, R. R. P.; McKenzie, R. H.; Coldea, R. *Phys. Rev. B* **2005**, *71*, 134422.
- [25] Foyevtsova, K.; Opahle, I.; Zhang, Y.-Z.; Jeschke, H. O.; Valentí, R. *Phys. Rev. B* **2011**, *83*, 125126.
- [26] Sala, M. M. et al. *New Journal of Physics* **2011**, *13*, 043026.
- [27] Ament, L. J. P.; van Veenendaal, M.; Devereaux, T. P.; Hill, J. P.; van den Brink, J. *Rev. Mod. Phys.* **2011**, *83*, 705–767.
- [28] Valiente, R.; Rodríguez, F. *Journal of Physics: Condensed Matter* **1998**, *10*, 9525–9534.
- [29] Marzari, N.; Mostofi, A. A.; Yates, J. R.; Souza, I.; Vanderbilt, D. *Rev. Mod. Phys.* **2012**, *84*, 1419–1475.
- [30] Ballhausen, C. J. *Introduction to Ligand Field Theory*; McGraw-Hill: New York, 1962.
- [31] Haverkort, M. W.; Zwierzycki, M.; Andersen, O. K. *Phys. Rev. B* **2012**, *85*, 165113.
- [32] Lu, Y.; Höppner, M.; Gunnarsson, O.; Haverkort, M. W. *Phys. Rev. B* **2014**, *90*, 085102.
- [33] Zaanen, J.; Sawatzky, G. A.; Allen, J. W. *Phys. Rev. Lett.* **1985**, *55*, 418–421.
- [34] Tcakaev, A. et al. *Phys. Rev. B* **2020**, *101*, 045127.
- [35] van den Brink, J. *New Journal of Physics* **2004**, *6*, 201–201.
- [36] Wohlfeld, K.; Nishimoto, S.; Haverkort, M. W.; van den Brink, J. *Phys. Rev. B* **2013**, *88*, 195138.
- [37] Ishihara, S. *Phys. Rev. B* **2004**, *69*, 075118.
- [38] Li, J.; Xu, L.; Garcia-Fernandez, M.; Nag, A.; Roberts, H. C.; Walters, A. C.; Liu, X.; Zhou, J.; Wohlfeld, K.; van den Brink, J.; Ding, H.; Zhou, K.-J. *Phys. Rev. Lett.* **2021**, *126*, 106401.
- [39] Towler, M. D.; Dovesi, R.; Saunders, V. R. *Phys. Rev. B* **1995**, *52*, 10150–10159.